Geophysical Prospecting, 2009, **57**, 355–365 doi: 10.1111/j.1365-2478.2008.00748.x

Comparison between the Fourier finite-difference method and the generalized-screen method

Jin-Hai Zhang[1]*, Wei-Min Wang[2] and Zhen-Xing Yao[1]

[1]*Institute of Geology and Geophysics, Chinese Academy of Sciences, PO Box 9825, Beijing 100029, China, and* [2]*Institute of Tibetan Plateau Research, Chinese Academy of Sciences, PO Box 2871, Beijing 100085, China*

Received February 2008, revision accepted June 2008

ABSTRACT

The Fourier finite-difference propagator and the generalized-screen propagator are two general high-order forms of one-way dual-domain methods. We compare these two propagators mainly on phase accuracy, computational efficiency and 3D extension. A comparison of phase accuracy shows that the high-order generalized-screen propagator is preferable to the Fourier finite-difference propagator for heterogeneous media with a weak velocity contrast and wide dip angle. With increasing velocity contrast, the accuracy improvement gained by the high-order generalized-screen propagator declines rapidly. The Fourier finite-difference propagator is more robust and flexible to lateral velocity variations than the generalized-screen propagator. The 2D Fourier finite-difference propagator is superior to the 2D generalized-screen propagator when the velocity contrast is stronger than 23%. Despite the two-way splitting error, the 3D Fourier finite-difference propagator is more accurate than the second-order generalized-screen propagator when the velocity contrast is stronger than 20% and is more accurate than the fourth-order generalized-screen propagator when the velocity contrast is stronger than 40%. Numerical experiments on the SEG/EAGE salt model demonstrate that the Fourier finite-difference propagator behaves better than the generalized-screen propagator when imaging steep salt boundary and faults beneath the salt body. Under the same hardware and software conditions, the computational cost of the Fourier finite-difference propagator in our implementation is greater than that of the second-order generalized-screen propagator but smaller than that of the third-order generalized-screen propagator. Compared with the Fourier finite-difference propagator, the generalized-screen propagator requires fewer grid points per wavelength and has more potential to improve running speed in the presence of a much faster Fourier transform. These analyses are applicable for both forward modelling and depth migration.

INTRODUCTION

One-way wave-equation migration is a rapidly growing tool for complex media imaging. Many methods have been developed during the last three decades, such as the finite-difference method (Claerbout 1985), Fourier method (Gazdag 1978) and dual-domain method (e.g., Stoffa *et al*. 1990; Wu 1994; Ristow and Rühl 1994; Jin, Wu and Peng 1999; de Hoop, Le Rousseau and Wu 2000; Le Rousseau and de Hoop 2001; Wu 2003). The finite-difference method can handle strong lateral velocity variations but it is dip-limited and has apparent numerical dispersions. The Fourier method is accurate up to 90° for homogeneous media and has almost no numerical dispersion but it has difficulty in handling lateral velocity variations.

The dual-domain method shuttles the wavefield between the space and wavenumber domains using fast Fourier transforms for each extrapolation step. The split-step Fourier method

*E-mail: zjh@mail.igcas.ac.cn

© 2009 European Association of Geoscientists & Engineers

(Stoffa *et al*. 1990) or phase-screen method (Wu 1994) is the simplest dual-domain method, where only time-delay correction is included. The Fourier finite-difference propagator (Ristow and Rühl 1994; Biondi 2002) and generalized-screen propagator (de Hoop *et al*. 2000; Le Rousseau and de Hoop 2001) are two general forms of the high-order dual-domain method.

The Fourier finite-difference method improves the accuracy by cascading an implicit finite-difference scheme to the split-step Fourier method. It can handle strong lateral velocity variations (e.g., salt-related model) and steep dips. However, it has three main disadvantages due to using an implicit finite-difference scheme, that is, low computational efficiency, splitting error for 3D exploration (Brown 1983; Zhang *et al*. 2008) and numerical dispersion for a coarse grid (Claerbout 1985).

Compared with the Fourier finite-difference method, the generalized-screen method directly extends the phase-screen method to complex media rather than using finite-difference correction, thus it has high efficiency, no splitting error and almost no numerical dispersion. In the presence of a large or strong velocity contrast, a high-order generalized-screen propagator is usually required, which undoubtedly increases computational cost. In addition, the generalized-screen propagator involves two Taylor expansions to the propagator (Le Rousseau and de Hoop 2001; Liu and Zhang 2006), thus the contribution of the high-order term becomes weak.

In 3D strongly heterogeneous media, the Fourier finite-difference propagator has high accuracy in in-line/cross-line direction but has low accuracy in diagonal directions caused by operator splitting (Brown 1983; Zhang *et al*. 2008). On the other hand, the Fourier finite-difference propagator degenerates into the phase-shift method in homogeneous media, which means there is no splitting error. However, it is still unclear whether and when the splitting error of the 3D Fourier finite-difference propagator would be bigger than the expansion error of the generalized-screen propagator. In addition, the generalized-screen propagator has several orders while the Fourier finite-difference propagator commonly-used has only one order. It is unclear whether the high-order generalized-screen propagator always has less computational cost than the Fourier finite-difference propagator. Therefore, it is difficult to select the most proper method in practical applications.

Cheng, Cheng and Toksöz (1996) presented a 3D error analysis of the phase-screen method. Huang and Fehler (1998) pointed out that the differences between the accuracy of the non-symmetrically and symmetrically split-step Fourier marching solutions are insignificant. The split-step Fourier propagator is shown to be accurate up to a wide angle (about 45°) for a weak velocity contrast (10%) under a relative error of 5%. Under large and strong velocity contrasts, a high-order propagator, such as the Fourier finite-difference propagator or generalized-screen propagator, is needed for forward modelling and depth migration. However, there are no thoroughly accurate analyses or a comparison of these two methods in the literature.

This paper compares the Fourier finite-difference method with the generalized-screen method mainly in three aspects: phase accuracy, computational efficiency and 3D extension. There are some skills to improve the performance of the Fourier finite-difference propagator and generalized-screen propagator, such as the 1/6 trick (Claerbout 1985) for the finite-difference scheme, optimized coefficients for the Fourier finite-difference propagator (Ristow and Rühl 1994; Xie and Wu 1999; Huang and Fehler 2000) and optimized coefficients for the generalized-screen propagator (Liu and Zhang 2006; Zhang and Liu 2007). We only discuss the most general form without any optimization or tricks to investigate the basic difference. After brief derivations of the Fourier finite-difference and generalized-screen operators, we analyse the flexibility and sensitivity on lateral velocity variations. Then, we discuss 3D extension and computational cost. Finally, we illustrate these theoretical analyses using impulse responses and numerical experiments.

METHODOLOGY

The Fourier finite-difference operator

The square-root operator of the one-way wave equation reads (Claerbout 1985):

$$k_z = \sqrt{\frac{\omega^2}{v^2} + \partial_{xx} + \partial_{yy}}, \tag{1}$$

where $\partial_{xx} = \frac{\partial^2}{\partial x^2}$, $\partial_{yy} = \frac{\partial^2}{\partial y^2}$, ω is the circular frequency and $v = v(x, y, z)$ is the velocity function. According to the perturbation approach (Wu 1994), a constant reference velocity function $v_0 = v_0(z)$ can be introduced to handle the homogeneous background for each depth step. The operator k_z for real velocity $v = v(x, y, z)$ can be expanded by the second-order Taylor expansion:

$$k_z \approx \frac{\omega}{v} + \frac{1}{2}\frac{v}{\omega}\left(\partial_{xx} + \partial_{yy}\right) - \frac{1}{8}\frac{v^3}{\omega^3}(\partial_{xx} + \partial_{yy})^2 \tag{2}$$

and similarly for the reference velocity $v_0 = v_0(z)$:

$$k_{z0} \approx \frac{\omega}{v_0} + \frac{1}{2}\frac{v_0}{\omega}\left(\partial_{xx} + \partial_{yy}\right) - \frac{1}{8}\frac{v_0^3}{\omega^3}\left(\partial_{xx} + \partial_{yy}\right)^2. \tag{3}$$

Substituting equations (2) and (3) into identical equation $k_z = k_{z0} + (k_z - k_{z0})$ and using a continued-fraction expansion, we obtain the popular Fourier finite-difference operator (Ristow and Rühl 1994; Biondi 2002):

$$k_z \approx k_{z0} + \omega \Delta s + \frac{b\left(\partial_{xx} + \partial_{yy}\right)}{1 + a\left(\partial_{xx} + \partial_{yy}\right)}, \tag{4}$$

where $k_{z0} = \sqrt{\omega^2/v_0^2 + \partial_{xx} + \partial_{yy}}$, $\Delta s = 1/v - 1/v_0$, $a = 0.25(v^2 + vv_0 + v_0^2)/\omega^2$ and $b = 0.5(v - v_0)/\omega$. On the right-hand side of equation (4), the first term handles the phase shift in the reference velocity (Gazdag 1978); the second term handles the time-delay correction for slowness perturbations (Stoffa *et al*. 1990; Wu 1994); and the third term handles the finite-difference correction for a large velocity contrast and wide dip angles (Ristow and Rühl 1994). The first two terms constitute the basics for most dual-domain methods, the so-called split-step Fourier method (Stoffa *et al*. 1990) or phase screen method (Wu 1994). The direct implementation of the implicit finite-difference scheme in the third term requires solving large sparse-matrix equations, which is extremely expensive. A practical way is to further split it into two independent operators by the two-way splitting technique (Brown 1983):

$$\frac{b\left(\partial_{xx} + \partial_{yy}\right)}{1 + a\left(\partial_{xx} + \partial_{yy}\right)} \approx \frac{b\partial_{xx}}{1 + a\partial_{xx}} + \frac{b\partial_{yy}}{1 + a\partial_{yy}}, \tag{5}$$

which can efficiently be solved as two cascaded tridiagonal systems. Thus, the two-way splitting Fourier finite-difference operator is:

$$k_z \approx k_{z0} + \omega \Delta s + \frac{b\partial_{xx}}{1 + a\partial_{xx}} + \frac{b\partial_{yy}}{1 + a\partial_{yy}}. \tag{6}$$

The error caused by equation (5) is called the splitting error. There are several approaches to reduce this error (Li 1991; Ristow and Rühl 1997; Wang 2001; Zhang *et al*. 2008) but we employ none of them in this paper for a fundamental comparison.

The generalized-screen operator

Substituting equations (2) and (3) into the square-root operator $k_z = k_{z0}\sqrt{1 - (\omega^2 s_0^2 - \omega^2 s^2)/k_{z0}^2}$ and using the Taylor expansion, we obtain:

$$k_z = k_{z0} + k_{z0} \sum_{n=1}^{\infty} a_n \left[\frac{\omega^2\left(s_0^2 - s^2\right)}{k_{z0}^2}\right]^n, \tag{7}$$

where $s = 1/v(x, y, z)$, $s_0 = 1/v_0(z)$ and a_n are binomial coefficients with the first four being $a_1 = -1/2$, $a_2 = -1/8$, $a_3 = -1/16$ and $a_4 = -5/128$. Considering:

$$\Delta s = s - s_0 = s_0 \sum_{n=1}^{\infty} a_n \left(1 - \frac{s^2}{s_0^2}\right)^n, \tag{8}$$

we obtain the generalized-screen operator:

$$k_z = k_{z0} + \omega \Delta s + k_{z0} \sum_{n=1}^{\infty} a_n \left(\frac{\omega^2 s_0^2 - \omega^2 s^2}{k_{z0}^2}\right)^n - \omega s_0 \sum_{n=1}^{\infty} a_n \left(1 - \frac{s^2}{s_0^2}\right)^n. \tag{9}$$

The first two terms on the right-hand side of equation (9) are the same as the first two terms of the Fourier finite-difference propagator shown in equation (6). In implementation, the exponential function of the third and fourth terms needs another Taylor expansion (i.e., $e^x \approx 1 + x$) (Le Rousseau and de Hoop 2001; Liu and Zhang 2006) that causes additional phase error. This error can be compensated on the whole by the normalizing operator proposed by De Hoop *et al*. (2000). Thus, for simplicity, we use equation (9) to evaluate the performance of the generalized-screen operator.

RELATIVE ERROR ANALYSES

To exhibit both the advantages and disadvantages of the methods, we numerically evaluate dispersion relations using relative phase error. First, we transform the spatial partial derivatives into the wavenumber domain using relations of $\partial_{xx} \Leftrightarrow -k_x^2$ and $\partial_{yy} \Leftrightarrow -k_y^2$, where k_x and k_y are transversal wavenumbers. We then represent transversal wavenumbers in terms of azimuth angle φ and dip angle θ as (Claerbout 1985; Li 1991):

$$k_x = \frac{\omega}{v}\sin\theta\cos\varphi \quad \text{and} \quad k_y = \frac{\omega}{v}\sin\theta\sin\varphi. \tag{10}$$

Thus, the relative phase error of the Fourier finite-difference propagator is defined as:

$$R_{FFD}(\varphi, \theta; v_0, v) = \frac{\left|k_z^{FFD} - \bar{k}_z\right|}{\bar{k}_z} \times 100\%, \tag{11}$$

where the accurate vertical wavenumber is:

$$\bar{k}_z = \frac{\omega}{v}\cos\theta \tag{12}$$

and the approximate vertical wavenumber is:

$$k_z^{FFD} \approx \bar{k}_{z0} + \omega \Delta s - \frac{bk_x^2}{1 - ak_x^2} - \frac{bk_y^2}{1 - ak_y^2}, \tag{13}$$

with $\tilde{k}_{z0} = \sqrt{\omega^2/v_0^2 - k_x^2 - k_y^2}$. Similarly, the relative phase error of the generalized-screen propagator is defined as:

$$R_{GSP}(\varphi, \theta; v_0, v) = \frac{\left|k_z^{GSP} - \tilde{k}_z\right|}{\tilde{k}_z} \times 100\%, \tag{14}$$

where the approximate vertical wavenumber is:

$$k_z^{GSP} \approx \tilde{k}_{z0} + \omega\Delta s + \omega \sum_{n=1}^{N} a_n \left(s_0^2 - s^2\right)^n \left(\frac{\omega^{2n-1}}{\tilde{k}_{z0}^{2n-1}} - \frac{1}{s_0^{2n-1}}\right). \tag{15}$$

Figure 1 shows the velocity contrast *versus* phase angle of the expanded square-root operator under relative error of 1% (a), 5% (b), 10% (c) and 20% (d), respectively. The velocity contrast is defined as $(v - v_0)/v \times 100\%$. A small velocity contrast denotes weak lateral velocity variations and a big one denotes strong lateral velocity variations. For example, it equals 0% for laterally homogenous media and equals 100% for extremely strong lateral velocity variations. The split-step Fourier method always shows the worst accuracy among all methods and the Fourier finite-difference propagator and generalized-screen propagator have different improvements on it for different velocity contrasts. In the large and strong velocity contrast area, the two-way splitting Fourier finite-difference propagator [see the solid line indicated by FFD90 for $\varphi = 90^\circ$ (i.e., the in-line/cross-line direction) and the dashed line indicated by FFD45 for $\varphi = 45^\circ$ (i.e., the diagonal direction)] has a much higher propagation angle than the generalized-screen propagator (see the solid lines indicated by numbers); however, the situation is the opposite in a weak velocity contrast area.

The fourth-order generalized-screen propagator (GSP4) is more attractive for the wide dip angle within the velocity contrast of 40% since both the in-line/cross-line and diagonal directions of the Fourier finite-difference propagator have a lower accurate dip angle. However, the lower order of the generalized-screen propagator has fewer advantages. For example, the GSP3 is more attractive only within the velocity contrast of 30% and the GSP2 only within 20%, as shown in Fig. 1(a).

For different relative errors shown in Fig. 1(a–d), the first four orders of the generalized-screen propagator are separate with each other in a weak velocity contrast area; whereas, they decline and get together gradually to the curve of the split-step Fourier method (dashed-dot line) with increasing velocity contrast. This indicates that the higher order of the generalized-screen propagator takes apparent effects for a weak heterogeneous media; whereas, the effect of the high-order generalized-screen propagator is considerably weak under a strong velocity contrast. Therefore, the Fourier

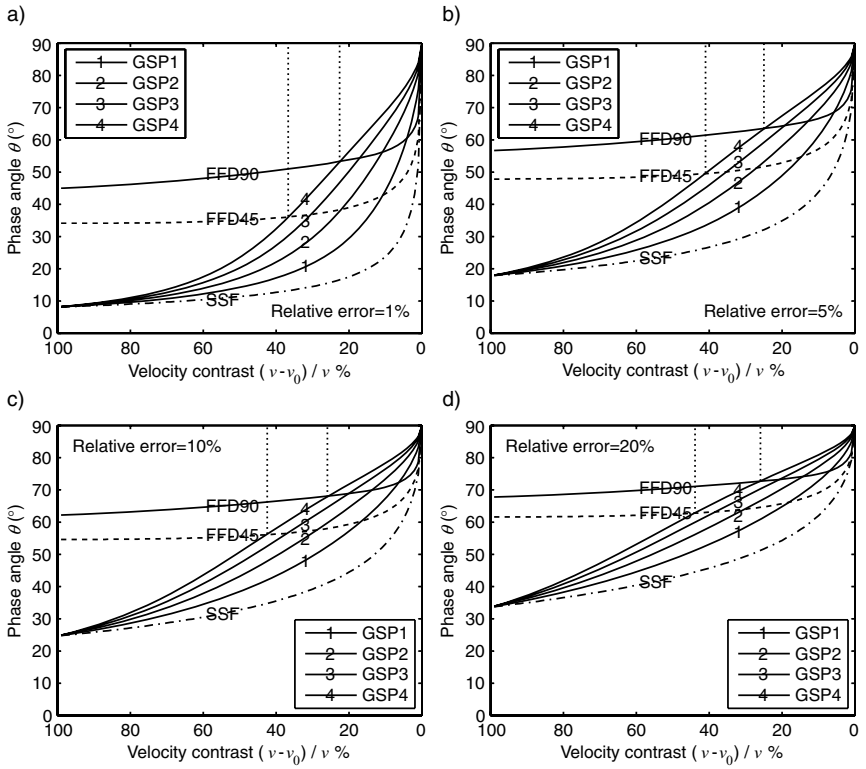

Figure 1 The velocity contrast versus the phase angle of the expanded square-root operator under a relative phase error of 1% (a), 5% (b), 10% (c) and 20% (d), respectively. The velocity contrast is defined as $(v - v_0)/v \times 100\%$. A small velocity contrast denotes weak lateral velocity variations and a big one denotes strong lateral velocity variations. The dashed-dot line denotes the split-step Fourier method; the solid line indicated by FFD90 and the dashed line indicated by FFD45 denote the Fourier finite-difference method in in-line/cross-line and diagonal directions, respectively; and the solid lines indicated by 1–4 denote the first four orders of the generalized-screen method, i.e., GSP1, GSP2, GSP3 and GSP4, respectively. For each sub-figure, above the line the error is larger than the chosen relative error, below it is smaller.

finite-difference propagator is more flexible than the generalized-screen propagator in handling large and strong velocity contrasts.

Under a relative error of 1%, the worst dip angle of the generalized-screen propagator is smaller than 10°; in contrast, the worst accuracy of the Fourier finite-difference propagator is greater than 35°. Under a relative error of 5%, the worst dip angle of the generalized-screen propagator is smaller than 20°; in contrast, the worst dip angle of the Fourier finite-difference propagator is greater than 47°. In addition, the curve of the generalized-screen propagator is steep on the whole; whereas, the curve of the Fourier finite-difference propagator is nearly horizontal, except for a very weak velocity contrast area. As shown in Fig. 1(a), the accurate dip angle of the GSP4 is about 70° under a velocity contrast of 10% but is only about 15° under a velocity contrast of 70% (e.g., salt model). In contrast, the accurate dip angle of the Fourier finite-difference propagator is always greater than 35° (45° for in-line direction) and varies only 10° under the same condition. Therefore, the generalized-screen propagator is sensitive to lateral velocity variations compared with the Fourier finite-difference propagator.

In Fig. 1, the points of intersection among the curves give the critical conditions of accuracy comparison. Note the curve of the 3D Fourier finite-difference propagator in the in-line/cross-line direction (FFD90) is the same as that of the 2D Fourier finite-difference propagator. Under a relative error of 1%, the 2D Fourier finite-difference propagator is superior to the GSP4 when the velocity contrast is stronger than 23%, as shown in Fig. 1(a). The diagonal direction of the Fourier finite-difference propagator (FFD45) has the most apparent splitting error, i.e., the worst accuracy among all azimuths. Despite this error, the 3D Fourier finite-difference propagator is more accurate than the GSP4 when the velocity contrast is stronger than 40%, as shown in Fig. 1(a–d). Under a relative error of 5%, the 3D Fourier finite-difference propagator is more accurate than the GSP1 when the velocity contrast is stronger than 15%, as shown in Fig. 1(b).

MODELLING IMPULSE RESPONSES

In this section, we illustrate the theoretical accuracy analyses by impulse responses. A 3D homogeneous medium is defined on a grid system of 256 × 256 × 128 with grid spacing of 10 m. The source is located at the centre of the upper surface. The traveltime is 450 ms with 2 ms sampling. The dominant frequency of the Ricker wavelet is 20 Hz and the maximum frequency is up to 80 Hz. The real velocity is $v = 2500$ m/s, with the reference velocity being $v_0 = 1000$ m/s (i.e., strong velocity contrast of $(v - v_0)/v = 60\%$), 1500 m/s (i.e., large

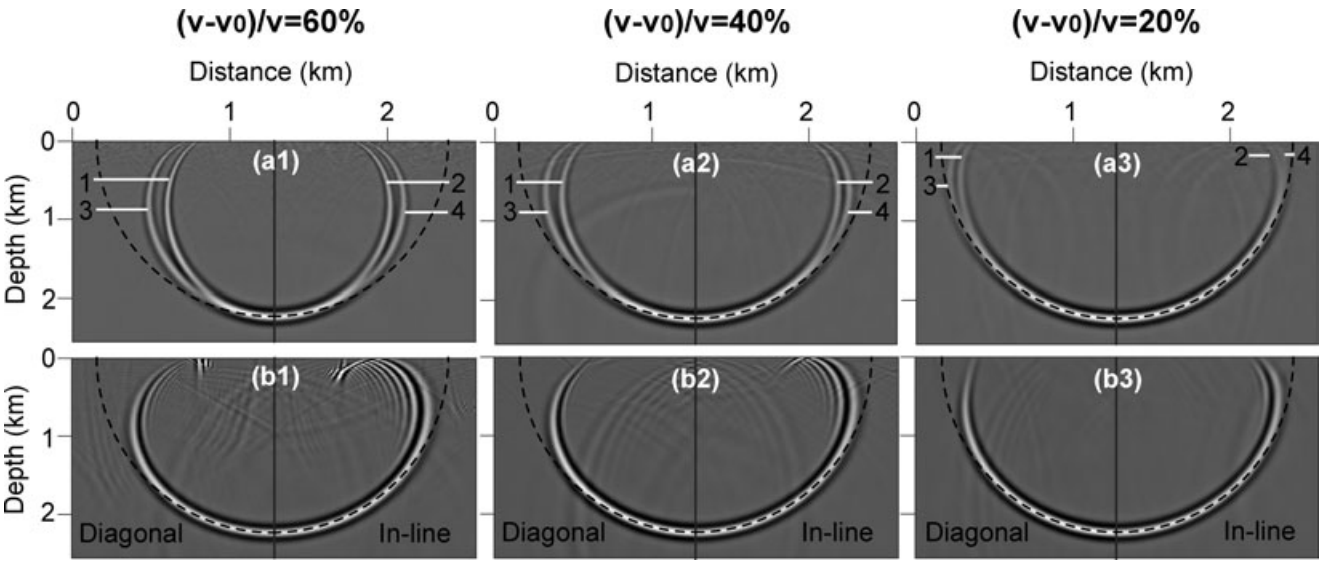

Figure 2 Vertical profiles at source location. The left, middle and right columns correspond to the velocity contrast $(v - v_0)/v \times 100\%$ of 60%(strong), 40%(large) and 20%(weak), respectively. The upper row denotes the generalized-screen propagator (a1–a3), where the vertical slices are superposed, i.e., the left side shows the GSP1 (indicated by 1) and GSP3 (indicated by 3), the right side shows the GSP2 (indicated by 2) and GSP4 (indicated by 4), respectively. The lower row denotes the two-way splitting Fourier finite-difference propagator, where each sub-picture (b1–b3) consists of two equivalent parts, i.e., the left side and right side show the vertical slice along the diagonal direction (indicated by diagonal) and along the in-line/cross-line direction (indicated by in-line), respectively. The dashed semicircle denotes the accurate position.

velocity contrast of $(v - v_0)/v = 40\%$) and 2000 m/s (i.e., weak velocity contrast of $(v - v_0)/v = 20\%$), respectively. We use a tapered boundary of 15 traces to each side of the transversal slab.

Figure 2 shows vertical slices of the generalized-screen method (a1–a3) and of the two-way splitting Fourier finite-difference method (b1–b3). The Fourier finite-difference propagator has apparent numerical dispersions and evanescent waves in a wide angle area in the presence of a strong velocity contrast, as shown in Fig. 2(b1) and 2(b2). In contrast, the generalized-screen propagator always has a clear background and less numerical artefacts than the Fourier finite-difference propagator.

It is obvious that the generalized-screen propagator has a very low accurate angle under the strong velocity contrast of 60% even for a high-order generalized-screen propagator (see Fig. 2(a1)) but has a very high accurate dip angle under the weak velocity contrast of 20% even for a low-order generalized-screen propagator (see Fig. 2(a3)). As shown in Fig. 2(b1–b3), in contrast, the Fourier finite-difference propagator always has a stable performance although the diagonal direction has a relatively lower accuracy (left-hand part) than the in-line/cross-line direction (right-hand part).

In Fig. 3, we show depth slices of the generalized-screen propagator in the same sub-picture to investigate contributions of the first four orders. Under a weak velocity contrast

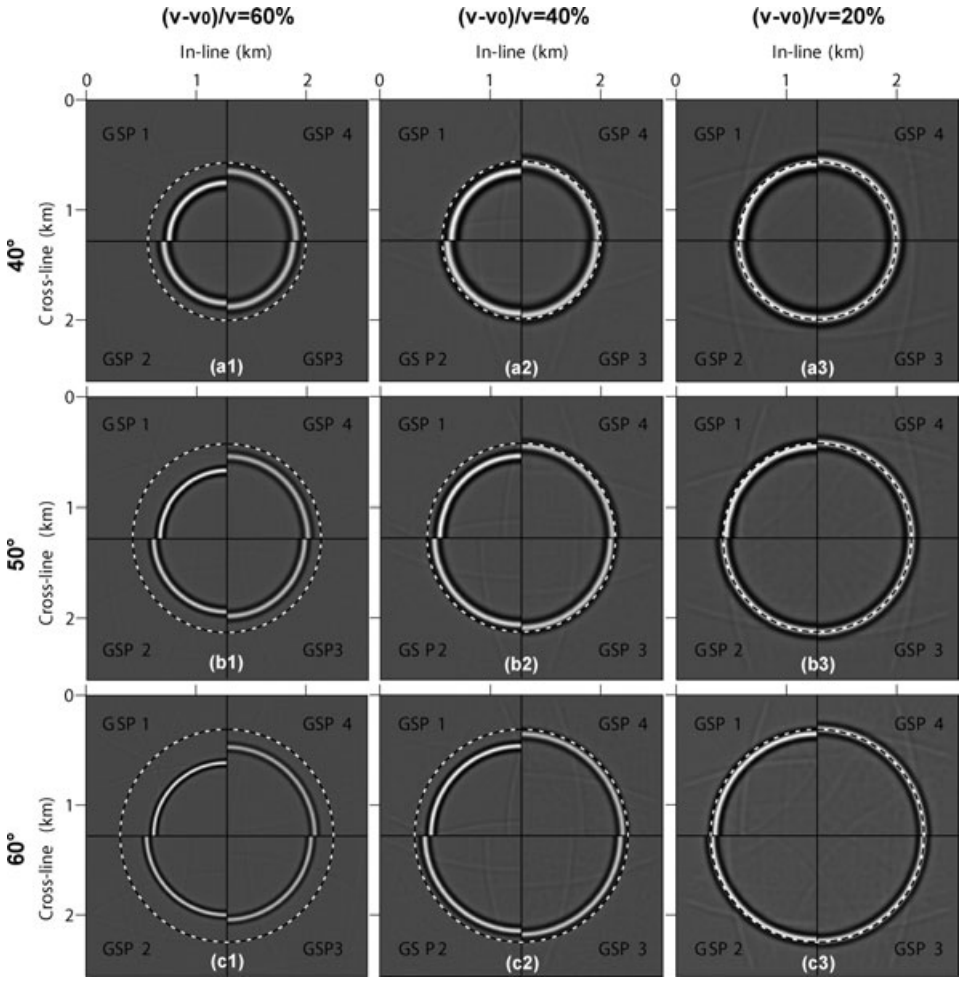

Figure 3 Depth slices from the first four orders of the generalized-screen propagator. The left, middle and right columns correspond to the velocity contrast $(v - v_0)/v \times 100\%$ of 60%, 40% and 20%, respectively. The upper, middle and bottom rows correspond to the dip angle of $40^\circ (z = 860$ m), $50^\circ (z = 720$ m) and $60^\circ (z = 560$ m), respectively. Each sub-picture consists of four equivalent parts, i.e., the left-upper quadrant shows GSP1, the left-bottom quadrant shows GSP2, the right-bottom quadrant shows GSP3 and the right-upper quadrant shows GSP4. The dashed circle denotes the accurate position.

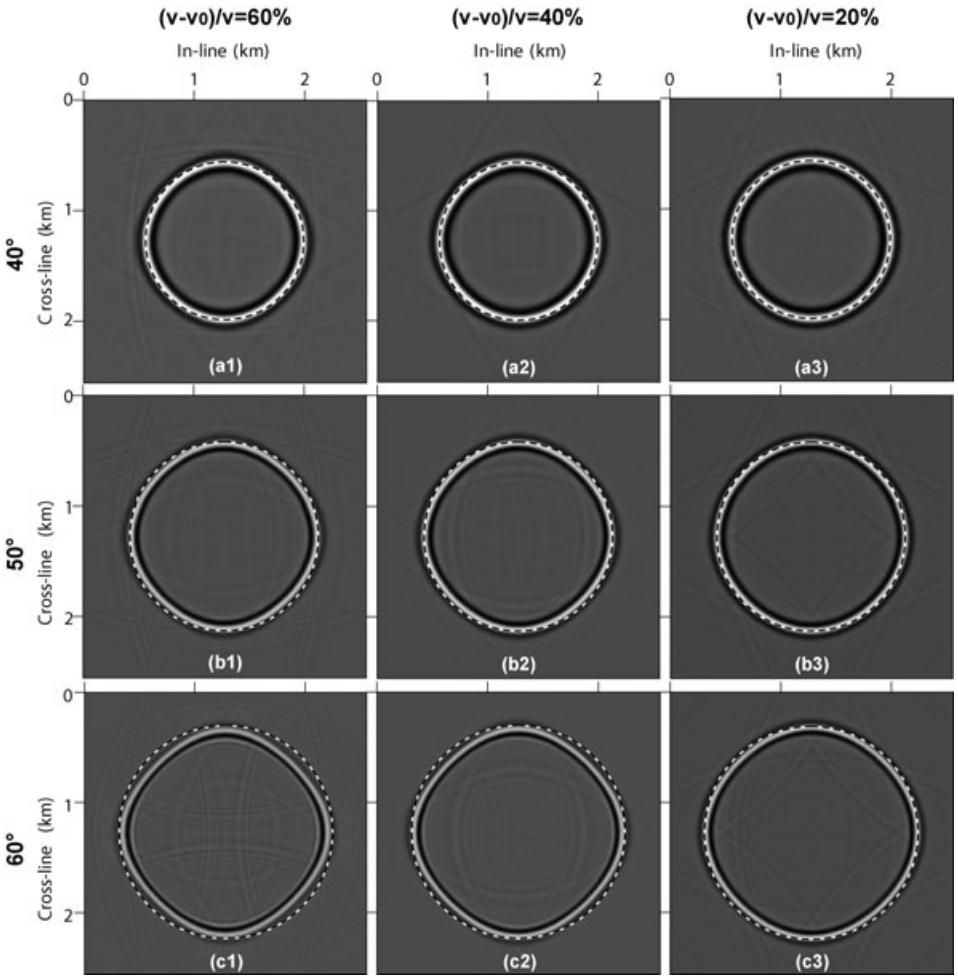

Figure 4 Depth slices from the two-way splitting Fourier finite-difference propagator. The left, middle and right columns correspond to the velocity contrast $(v - v_0)/v \times 100\%$ of 60%, 40% and 20%, respectively. The upper, middle and bottom rows correspond to the dip angle of $40^\circ (z = 860$ m), $50^\circ (z = 720$ m) and $60^\circ (z = 560$ m), respectively. The dashed circle denotes the accurate position.

(e.g., $(v - v_0)/v = 20\%$), the generalized-screen propagator, except for the GSP1, has a very high accuracy whether for a low dip angle, as shown in Fig. 3(a3), or for higher dip angles, as shown in Figs 3(b3) and 3(c3). Unfortunately, this advantage decays rapidly under a large or strong velocity contrast, as shown in Figs 3(a1), 3(b1) and 3(c1). For example, the GSP4 has poor accuracy for a wide dip angle under the large velocity contrast of 40%, as shown in Fig. 3(c2); in addition, the GSP4 has a poor accuracy for low dip angles under a strong velocity contrast of 60%, as shown in Figs 3(a1) and 3(b1). From Figs 2 and 3, we see that the Fourier finite-difference propagator is more flexible and less sensitive to velocity contrast compared with the generalized-screen propagator.

The impulse responses of the generalized-screen propagator shown in Fig. 3 are invariable along different azimuthal directions. In contrast, the impulse responses of the Fourier finite-difference propagator shown in Fig. 4 are not a perfect circle as expected but a smoothed diamond. This error is introduced by the two-way splitting approximation of the 3D finite-difference term, i.e., equation (5). It reduces the wide-angle accuracy at azimuths other than in-line and cross-line directions. As shown in Fig. 4, the splitting error is slight for a low dip angle (a1–a3) but increases gradually with a much higher dip angle (b1–b3 and c1–c3). This error becomes significant for a wide angle (e.g., 60° in Fig. 4(c1)) in the presence of a strong velocity contrast $(v - v_0)/v = 60\%$.

Under large and strong velocity contrasts, the Fourier finite-difference propagator is very accurate despite the two-way splitting error when comparing its slices, shown in Figs 4(a1), 4(b1) and 4(c1), with that of the generalized-screen propagator, shown in Figs 3(a1), 3(b1) and 3(c1). Furthermore,

the in-line/cross-line direction is always close to the accurate position (indicated by the dashed circle). Therefore, the 3D Fourier finite-difference propagator is more accurate than the 3D generalized-screen propagator on the whole in the presence of large and strong velocity contrasts, although it has the worst accuracy in the diagonal direction.

In fact, these impulse responses shown in Figs 3 and 4 are consistent with the previous accuracy analyses shown in Fig. 1. For example, the accurate angle of the GSP1 under the velocity contrast of 20%, i.e., the solid line indicated by 1 in Fig. 1(a), is slightly lower than 40° while others are higher than 40°; these can be verified by Fig. 3(a3). For another example, the 3D Fourier finite-difference propagator has apparent splitting error in the diagonal direction (see the dashed line in Fig. 1(a)) but is accurate in the in-line/cross-line direction for a dip angle of 50° under a velocity contrast of 40% [(see the solid line indicated by FFD90 in Fig. 1(a)]; these can be verified by Fig. 4(b2). Our impulse responses can also be verified by results gained by Le Rousseau and de Hoop (2001) and by Liu and Zhang (2006).

Under the same hardware and software conditions, the Fourier finite-difference propagator spends 476.3 CPU seconds, while the first four orders of the generalized-screen propagator spend 370.7, 443.1, 517.5 and 597.3 CPU seconds, respectively. Obviously, the computational cost of the generalized-screen propagator increases linearly with the order used and the computational cost of the Fourier finite-difference propagator lies between that of the GSP2 and GSP3. There is no dip filter, since all methods are stable and produce clear images. A hybrid radix fast Fourier transform, which is one of the fastest algorithms, is used in our code.

MIGRATION FOR SEG/EAGE SALT

To verify the capabilities of the Fourier finite-difference propagator and generalized-screen propagator on imaging 3D complex structures, we test on the zero-offset records (Ober *et al.* 1997) of the SEG/EAGE 3D salt model (Aminzadeh *et al.* 1996). We extract every other grid along in-line and cross-line directions from the original data. That is, the 3D grid system used here is of 250 × 250 × 210 with the spacings of 40 m along the transversal direction and 20 m along the depth direction. The frequency range for migration is from 0 to 60 Hz. We use a tapered boundary of 5 traces to each side of the transversal slab.

In the diagonal direction (i.e., $x = y$), the two-way splitting Fourier finite-difference propagator has the worst accuracy among all azimuths. Figure 5 shows the vertical slice of the

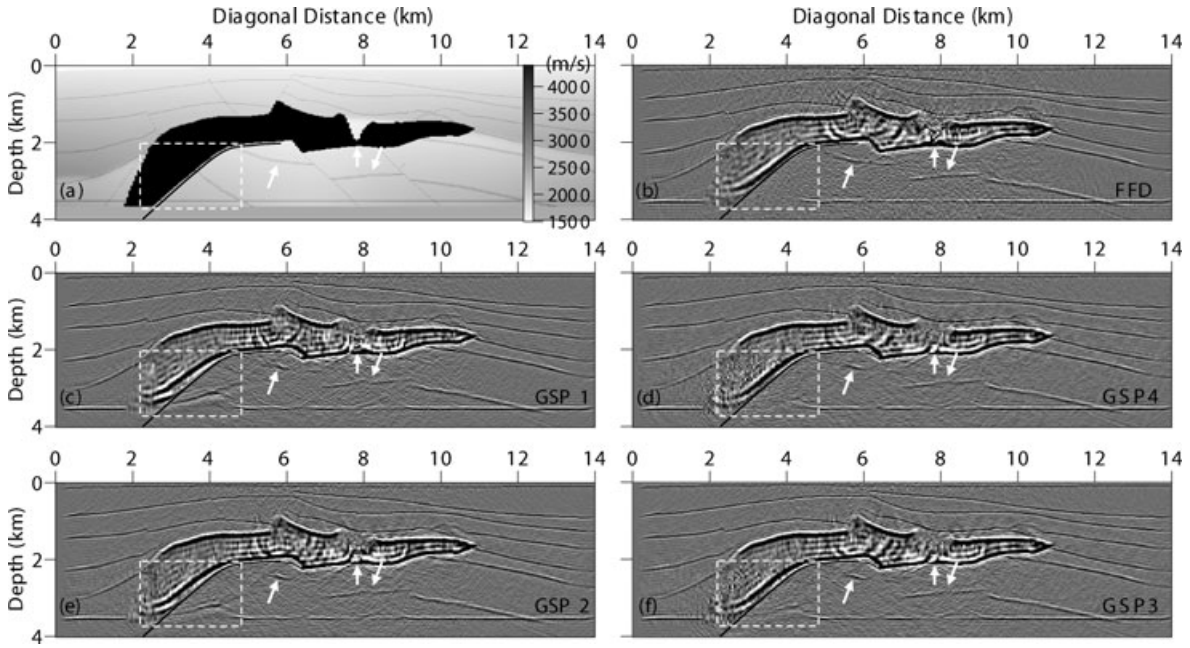

Figure 5 The vertical profile along the diagonal direction of the SEG/EAGE 3D salt model (a) and corresponding images obtained by the two-way splitting Fourier finite-difference propagator (b), GSP1 (c), GSP4 (d), GSP2 (e) and GSP3 (f), respectively. The solid line denotes the bottom salt boundary. The transversal and depth directions have the same scale.

model and images along the diagonal direction. It is obvious that each method can well image small-angle structures but poorly image the left boundary of the salt root. The latter may be caused by an aperture problem, since the reflected wavefields are out of the receiver range. Since all slices are shown in the same scale along the depth and transversal directions, we see that the left boundary of the salt root has, at least, a 60° dip angle.

Both the steep salt boundary (indicated by the solid line) and structures under the salt body (indicated by white arrows) are well imaged by the two-way splitting Fourier finite-difference propagator, as shown in Fig. 5(b). Although each higher order of generalized-screen propagator can improve the image, the result is not as good as that of the Fourier finite-difference propagator even for the GSP4, as shown in Fig. 5(d). For detailed comparison, images within the rectangular areas in Fig. 5 are shown in Fig. 6. Obviously, the two-way splitting Fourier finite-difference propagator gives the best images among all methods listed. There are apparent artefacts in the ellipse area for the low-order generalized-screen propagator (GSP1 and GSP2), as shown in Fig. 6(c) and 6(e). Figure 7 shows the horizontal slice of the velocity at depth $z = 2140$ m (a) and its migration images. In the ellipse area of Fig. 7, the two-way splitting Fourier finite-difference propagator well focuses the steep salt boundary (b) compared with those obtained using GSP (c-f).

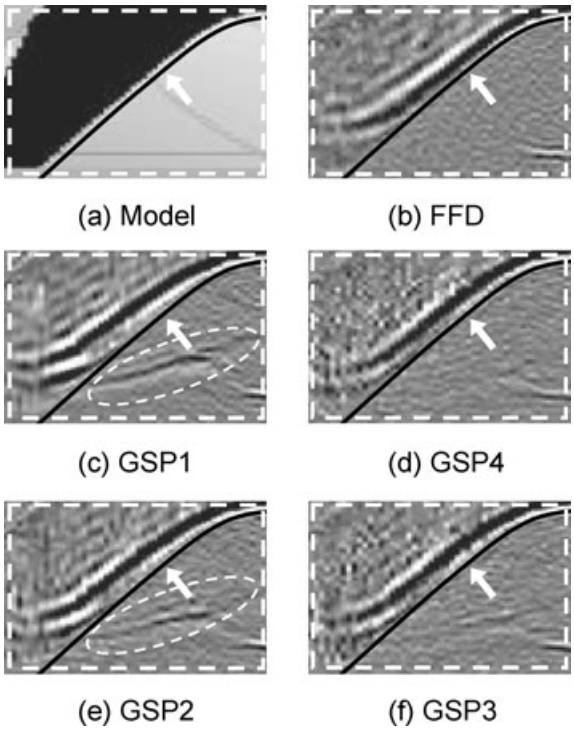

Figure 6 Comparison of the local details within the rectangular areas in Fig. 5. The solid line denotes the bottom salt boundary.

Under the same hardware and software conditions, the Fourier finite-difference propagator spends 587.7 CPU seconds, while the first four orders of the generalized-screen propagator spend 466.3, 549.3, 630.2 and 1285.0 CPU seconds, respectively. The computational cost of the Fourier finite-difference propagator again is between those of GSP2 and GSP3. We use a 60° dip filter in the wavenumber domain for all methods to damp the strong artefacts especially for GSP4. However, apparent noises still exist in the image obtained using GSP4. In addition, the computational cost of GSP4 is double that of GSP3, which is abnormal compared with the linear cost relation shown in the experiment of impulse responses. These indicate that GSP4 may have a stability problem in the presence of a strong velocity contrast although the normalizing operator is used.

DISCUSSIONS

From the above theoretical analyses and numerical experiments, we see that the main disadvantages of the Fourier finite-difference propagator, i.e., low computational efficiency, splitting error for 3D exploration and numerical dispersion for a coarse grid, are sometimes overstated when comparing with the generalized-screen propagator. First, the two-way splitting Fourier finite-difference propagator is not as expensive as usually considered since its computational cost is less than that of the third-order generalized-screen propagator. Second, the two-way splitting Fourier finite-difference propagator is more accurate than the generalized-screen propagator under large and strong velocity contrasts although the splitting error may reduce the wide-angle accuracy. Finally, the Fourier finite-difference propagator has fewer numerical artefacts than the generalized-screen propagator when imaging the SEG/EAGE salt model although it is not the case in impulse responses. If we could reduce the splitting error without too much cost (e.g., Zhang *et al*. 2008), the Fourier finite-difference propagator would be greatly superior to the fourth-order generalized-screen propagator when the velocity contrast is bigger than 23% as in the 2D case rather than 40% in the 3D case.

Most of the computational cost of the generalized-screen propagator is related to the operator order and speed of the Fourier transform. Thus, the generalized-screen propagator has a potential advantage that its efficiency can be highly improved with a much faster Fourier transform. Compared with the generalized-screen propagator, the Fourier

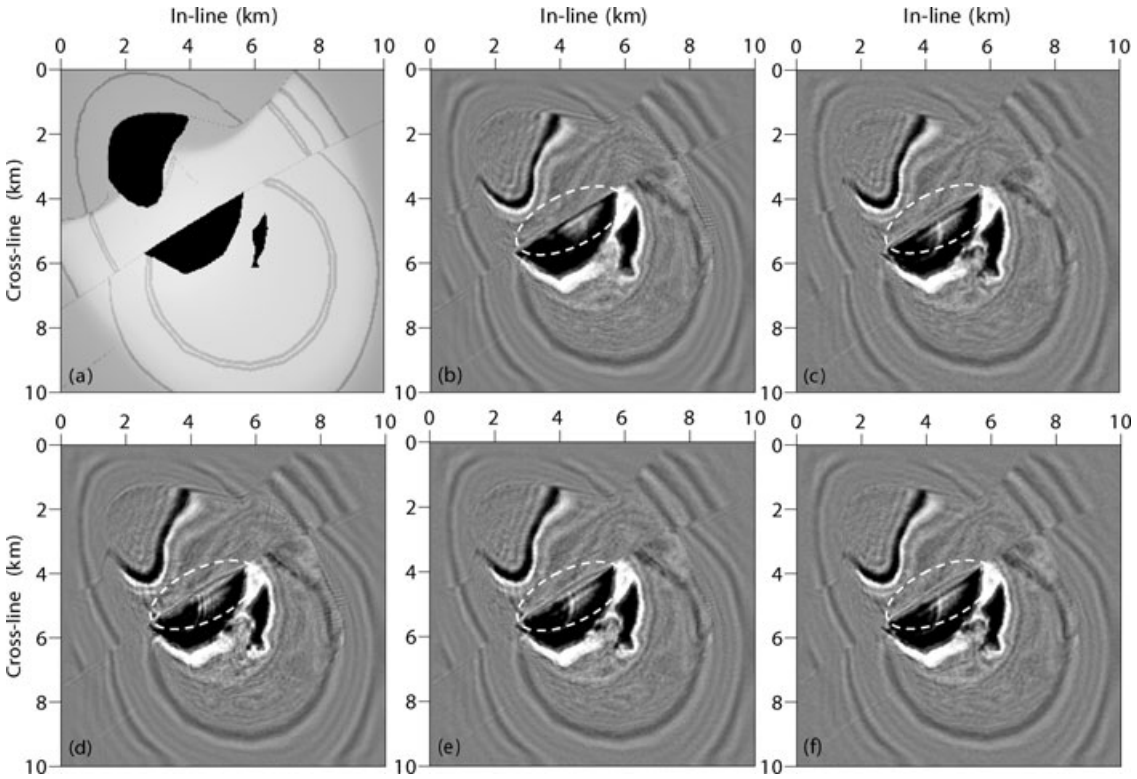

Figure 7 Depth slice of the SEG/EAGE 3D salt model (a) and corresponding images obtained using the two-way splitting Fourier finite-difference propagator (b), GSP4 (c), GSP1 (d), GSP2 (e) and GSP3 (f), respectively. The depth slice is at the depth of $z = 2140$ m.

finite-difference propagator has fewer benefits with a much faster Fourier transform, since the main computational cost of the Fourier finite-difference propagator lies on an implicit finite-difference scheme which is difficult to be further accelerated. In addition, the generalized-screen propagator has no splitting error and almost no numerical dispersion; thus an attractive propagator can be produced if some improvements were made on the phase accuracy for large or strong velocity contrasts.

We only use zero-offset data on a salt-related model in our experiments, where there are few steep dips. In the pre-stack data, the paths connecting the reflectors to the sources and receivers are usually at a wide angle (Biondi 2002). Thus, the efficient wide-angle propagator is crucial and would take more effects.

CONCLUSIONS

Without any tricks or optimized parameters, we compare the two-way splitting Fourier finite-difference method and the generalized-screen method to investigate the fundamental differences. The computational cost of the Fourier finite-difference propagator in our experiment is between those of the second and third-order generalized-screen propagators. Based on relative phase errors, our accuracy analyses show that the generalized-screen propagator has a higher accurate propagation angle than the Fourier finite-difference propagator when the velocity contrast $(v-v)/v \times 100\%$ is weaker than 40% for the fourth-order generalized-screen propagator, 30% for the third-order generalized-screen propagator, 20% for the second-order generalized-screen propagator and 10% for the first-order generalized-screen propagator, respectively.

However, the Fourier finite-difference propagator is superior to each order of generalized-screen propagator when the velocity contrast is stronger than 40% despite the two-way splitting error. Compared with the generalized-screen propagator, the Fourier finite-difference propagator is more flexible and less sensitive to the lateral velocity contrast. Impulse responses and migration results on the SEG/EAGE salt model show that the two-way splitting Fourier finite-difference propagator can well image steep dips and faults under the salt body even in the diagonal direction; whereas, the generalized-screen propagator can handle only complex structures without the disturbance of a large and strong velocity contrast. When

considering the numerical dispersion, computational cost and accurate dip angle, the generalized-screen propagator is more suitable to weak heterogeneous media while the Fourier finite-difference propagator is more attractive for large and strong heterogeneous media.

ACKNOWLEDGEMENTS

We thank Dr Jianfeng Zhang for helpful discussions. We are grateful to editors and anonymous reviewers for valuable comments and suggestions. This research was supported by the Knowledge Innovation Program of the Chinese Academy of Sciences (Grant No.KZCX2-YW-101), by China Postdoctoral Science funded project and by the Special Foundation for Excellent Doctoral Thesis and President Prize, Chinese Academy of Sciences.

REFERENCES

Aminzadeh F., Burkhard N., Long J., Kunz T. and Dulcos P. 1996. Three dimensional SEG/EAGE models – An update. *The Leading Edge* **15**, 131–134.

Biondi B. 2002. Stable wide-angle Fourier finite-difference downward extrapolation of 3D wavefields. *Geophysics* **67**, 872–882.

Brown D.L. 1983. Applications of operator separation in reflection seismology. *Geophysics* **48**, 288–294.

Cheng N., Cheng C.H. and Toksöz M.N. 1996. Error analysis of phase screen method in 3-D. *Geophysical Research Letters* **23**, 1841–1844.

Claerbout J.F. 1985. *Imaging The Earth's Interior*. Blackwell.

Gazdag J. 1978. Wave equation migration with the phase-shift method. *Geophysics* **43**, 1342–1351.

de Hoop M.V., Le Rousseau J.H. and Wu R.S. 2000. Generalization of the phase-screen approximation for the scattering of acoustic waves. *Wave Motion* **31**, 285–296.

Huang L.J. and Fehler M.C. 1998. Accuracy analysis of the split-step Fourier propagator: implications for seismic modeling and migration. *Bulletin of the Seismological Society of America* **88**, 18–29.

Huang L.J. and Fehler M.C. 2000. Globally optimized Fourier finite-difference migration method. 70th SEG meeting, Calgary, Canada, Expanded Abstracts, 802–805.

Jin S., Wu R.S. and Peng C. 1999. Seismic depth migration with pseudo-screen propagators. *Computational Geosciences* **3**, 321–335.

Le Rousseau J.H. and de Hoop M.V. 2001. Modeling and imaging with the scalar generalized-screen algorithms in isotropic media. *Geophysics* **66**, 1551–1568.

Li Z. 1991. Compensating finite-difference errors in 3D migration and modeling. *Geophysics* **56**, 1650–1660.

Liu L. and Zhang J. 2006. 3D wavefield extrapolation with optimum split-step Fourier method. *Geophysics* **71**, T95–T108.

Ober C.C., Oldfield R.A., Womble D.E. and Mosher C.C. 1997. Seismic imaging on massively parallel computers. 67th SEG meeting, Dallas, Texas, USA, Expanded Abstracts, 1418–1421.

Ristow D. and Rühl T. 1994. Fourier finite-difference migration. *Geophysics* **59**, 1882–1893.

Ristow D. and Rühl T. 1997. 3-D implicit finite-difference migration by multiway splitting. *Geophysics* **62**, 554–567.

Stoffa P.L., Fokkema J.T., de Luna Freire R.M. and Kessinger W.P. 1990. Split-step Fourier migration. *Geophysics* **55**, 410–421.

Wang Y. 2001. ADI plus interpolation: Accurate finite-difference solution to 3D paraxial wave equation. *Geophysical Prospecting* **49**, 547–556.

Wu R.S. 1994. Wide-angle elastic wave one-way propagation in heterogeneous media and an elastic wave complex-screen method. *Journal of Geophysics Research* **99**, 751–766.

Wu R.S. 2003. Wave propagation, scattering and imaging using dual-domain one-way and one-return propagators. *Pure and Applied Geophysics* **160**, 509–539.

Xie X.B. and Wu R.S. 1999. Improve the wide-angle accuracy of screen propagator for elastic wave propagation. 69th SEG meeting, Houston, Texas, USA, Expanded Abstracts, 1863–1866.

Zhang J. and Liu L. 2007. Optimum split-step Fourier 3D depth migration: Developments and practical aspects. *Geophysics* **72**, S167-S175.

Zhang J.H., Wang W.M., Fu L.Y. and Yao Z.X. 2008. 3D Fourier finite-difference migration by ADI plus interpolation. *Geophysical Prospecting* **56**, 95–103.